Improved properties of TiAlN coatings through the multilayer structure

A. Rizzo [a],*, L. Mirenghi [a], M. Massaro [a], U. Galietti [b], L. Capodieci [a], R. Terzi [a], L. Tapfer [a], D. Valerini [a]

[a] ENEA — Italian National Agency for New Technologies, Energy and the Sustainable Economic Development, Technical Unit for Materials Technologies, Brindisi Research Center, S.S. 7 Appia km. 706, 72100 Brindisi, Italy
[b] Politecnico di Bari, DIMEG — Dipartimento di Ingegneria Meccanica e Gestionale, Viale Japigia 182, I-70126 Bari, Italy

ABSTRACT

TiAlN/AlN multilayers are attracting great interest for the possibility to modulate their mechanical and tri-bological properties through the variation of multilayer design. In this work TiAlN single layer, TiAlN/AlN intermixed-multilayer and nano-multilayer were prepared using a reactive magnetron sputtering system starting from targets of TiAl and Al. The aim is to analyze how the multilayer design affects the thermal and tribological properties of the coatings. The microstructure of as-deposited and annealed films has been studied using X-ray diffraction. The chemical composition has been deduced by XPS analyses. Thermal behavior was assessed by means of differential thermal analysis (DTA) and thermogravimetric analysis (TGA), while mechanical properties have been investigated by wear tests.

© 2013 The Authors. Published by Elsevier B.V. Open access under CC BY-NC-ND license.

1. Introduction

Surface coating on tools can confer them a high wear resistance, an increased surface hardness at high temperatures and create a chemical barrier for diffusion or reaction between the tool and the working-piece, thus reducing tool wear [1,2]. Therefore, the demand to develop new wear resistant hard coatings with good thermal stability has become crucial to enhance tool life as machining speed increases [3]. The first coating successfully used in steel machining industry and still employed for its attractive bright gold color, is titanium nitride (TiN). However, its use at elevated temperature is restricted due to its poor chemical stability and it has been replaced by TiAlN in several applications [4]. It has been shown that the mechanical properties of TiAlN material are strongly dependent on its chemical composition [5,6]. A coating with a composition of $Ti_{0.35}Al_{0.65}N$ shows a slightly higher oxidation resistance than $Ti_{0.62}Al_{0.38}N$. On the other hand, an increase of Al amount in the TiAlN coating, such as in $Ti_{0.19}Al_{0.81}N$, revealed a worse oxidation resistance, similar to that found for AlN [7]. Then, improvements of TiAlN coating properties can be obtained optimizing the Al content, the microstructure and the crystal orientation. Multi-layer coatings and superlattices are the most widely employed to provide a better alternative to single layer structures [8,9]. These systems allow to suitably combine different materials, selected to ensure that the properties of the resulting coating are optimized for the specific application required [10–12]. Then, once selected the proper materials, an accurate engineering of the coating structure is necessary to identify the powerful system with the best functional properties. In this work TiAlN and AlN were chosen as basic materials and combined under different architectures, namely, nano-multilayer, intermixed-multilayer and single layer structures. All coatings were deposited by magnetron sputtering. Afterwards, microstructure, chemical composition, thermal stability and mechanical properties of the single layer and the multilayers were investigated by using a combination of X-ray diffraction (XRD), X-ray photoelectron spectroscopy (XPS), thermal analysis TGA (thermogravimetric analysis) and DTA (differential thermal analysis) and tests of wear and friction. Finally, the worn surfaces of these coatings were analyzed by means of scanning electron microscopy (SEM) and energy dispersive spectroscopy (EDS).

2. Experimental details

TiAlN and TiAlN/AlN multilayered coatings were deposited on silicon and WC–6%Co using a multi-cathode reactive RF magnetron sputtering system.

TiAl (99.95%) and Al (99.9%) targets were sputtered in high purity plasma of Ar (99.999%) and N_2 (99.999%). The composition of the TiAl target was approximately 50:50 in atomic percentage. For all the experiments, the power densities were approximately 3.88 and 1.94 W/cm^2 for the TiAl and Al targets, respectively.

The coatings were deposited under a base pressure of 2.0×10^{-5} Pa and a working total pressure of Ar + N_2 gas equal to 4.0 Pa. The flow rates of N_2 and Ar were separately controlled by two mass flow controllers. The flow rate ratio of N_2 and Ar + N_2 was fixed at 5%.

* Corresponding author. Tel.: +39 0831201428.
 E-mail address: antonella.rizzo@enea.it (A. Rizzo).

The substrates were cleaned in acetone and isopropyl alcohol by ultrasonic cleaning. The substrates were subsequently etched in situ by Ar$^+$ ion bombardment for 45 min, obtained by applying a RF bias of −20 V to the substrate at an argon pressure of 6.0×10^{-1} Pa. The coatings were deposited at a substrate temperature of 150 °C.

A Ti interlayer was deposited on the WC–6%Co substrates to improve the adhesion of the coatings. Coatings with controlled layer thicknesses were deposited using a stepper motor connected to the substrate holder through a rotary feed. The substrate was moved in circular motion between the two sputtering targets using the stepper motor. The substrate was kept underneath each target for a well predetermined time to achieve the required multilayer thickness.

The multilayers were realized with two different methods of alternation of TiAlN and AlN layers, i.e. continuously deposited with both targets (TiAl and Al) turned on and the substrate rotating and passing under each of the target (TiAlN/AlN-i, where "i" stands for "intermixed") or, alternatively, deposited with only one target turned on and with the power switching between the two targets at each cycle (TiAlN/AlN-n, where "n" stands for "nano-multilayer"). Look at Fig. 1 which shows schematically in the deposition system the relative position of the sputtering sources and the substrate table. In this way, it is easier to understand how the deposition was carried out for samples TiAlN/AlN-i and TiAlN/AlN-n.

The multilayer period is about 4.5 nm. Coatings deposited on silicon substrates with thickness of about 40 nm (corresponding to 9 periods in multilayered films) were used for structural, chemical and thermal stability studies, while coatings deposited on WC–6%Co substrates with thickness of approximately 2.2 μm (corresponding to 500 periods in multilayered films) were used for wear tests.

The X-ray diffraction and reflectivity experiments were carried out by using an X-ray diffractometer in parallel beam geometry (Philips MPD PW1880, 3 kW generator) optimized for small-angle scattering measurements. For all the measurements $Cu_{K\alpha}$-radiation ($\lambda_{CuK\alpha} = 0.154186$ nm) was used. The X-ray diffraction measurements (XRD) were performed at glancing incidence angle (with fixed incidence angle $\omega_i = 1.0°$) in a range between 5° and 85°. Specular (ω, 2θ) scans (XSR) were acquired at the grazing angle of incidence of the X-rays equal to the exit angle 2θ measured in the range between 0° and 9° with a step size of 0.01°.

For X-ray photoelectron spectroscopy (XPS) studies, samples were analyzed by AXIS Ultra DLD KRATOS using an Al Kα monochromatic X-ray source at 600 W. Survey scans were acquired at a pass energy of the analyzer equal to 160 eV, while narrow scans were acquired with a pass energy of 20 eV. All spectra were recorded from an analysis area of 700×300 μm^2, while depth profiling was performed all along the films' thickness using a coronene ($C_{24}H_{12}^+$) organic source as sputtering source [13]. The energy of the $C_{24}H_{12}^+$ gun was 8 keV,

sputtering the samples at 65° respect to the surface normal. The use of this organic source ensures the absence of alteration of the chemical composition and bonds along the specimen thickness, unlike conventional Ar$^+$ sources. In the depth profiles, a normalization respect to the C1s signal has been operated, because the C1s signal detected inside the films was due to the implanted carbon from coronene. During spectrum acquisition the charge neutralizer was always on. "CasaXPS" software [14] was used both for quantitative peak fitting on narrow spectra of Ti 2p, Al 2p, N1s and O 1s regions and on survey spectra to built up the depth profiling.

Differential thermal analysis (DTA) with thermogravimetry (TGA) was performed in a calibrated Netzsch-STA 409C from room temperature (RT) up to 1300 °C with a heating rate of 20 °C/min in flowing Ar (99.999% purity, 20 sccm flow rate) and synthetic air (79% N$_2$, 21% O$_2$, 20 sccm flow rate) to mimic application conditions. Every DTA curve was corrected using as baseline the second scan performed on the same material. The annealing process of the coatings was performed in vacuum (base pressure below 5 mPa) with heating and cooling rates of 20 °C/min at temperatures of 700, 800, 900, and 1000 °C on silicon substrates. The same coatings have been analyzed by XRD in order to support the DTA results.

A pin-on-disk wear method was used to investigate the wear resistance of the coatings. A bearing steel ball, 5.5 mm in diameter, was adopted as the stationary pin. A normal load of 1 N was applied.

The sliding speed was 0.2 m/s on the circular track, for 500 rotations of the sample. The test temperatures were 30 °C and 400 °C and the relative humidity was kept at 60%. The wear time was 40 min for each test. Three friction tests were conducted for each specimen and for every wear scan five measurements of the total wear volume were performed at different points of the wear path and their average values are reported. The wearing morphology of the films was investigated by scanning electron microscope (SEM) XL40 Philips in plan view and significant areas inside and outside the wear tracks were examined by energy dispersive spectroscopy analyzer (EDS).

3. Results

3.1. Structure of coatings

Fig. 2 presents the X-ray diffractograms of TiAlN, TiAlN/AlN-n and TiAlN/AlN-i coatings. The TiAlN/AlN-n coating (see Fig. 2 in the middle) shows the characteristic peak of the (101) direction of h-AlN s.g. P6$_3$mc (JCPDS card #87-1054) at $2\theta = 38.29°$. Two broad peaks, centered at ~35° and ~40.2°, not expected, can be attributed to the hexagonal phase of Ti$_2$AlN (JCPDS card #18-0070). In addition there are two peaks related to the (111) and (200) directions of the cubic phase of TiAlN. Experimental investigations show that Ti$_{1-x}$Al$_x$N
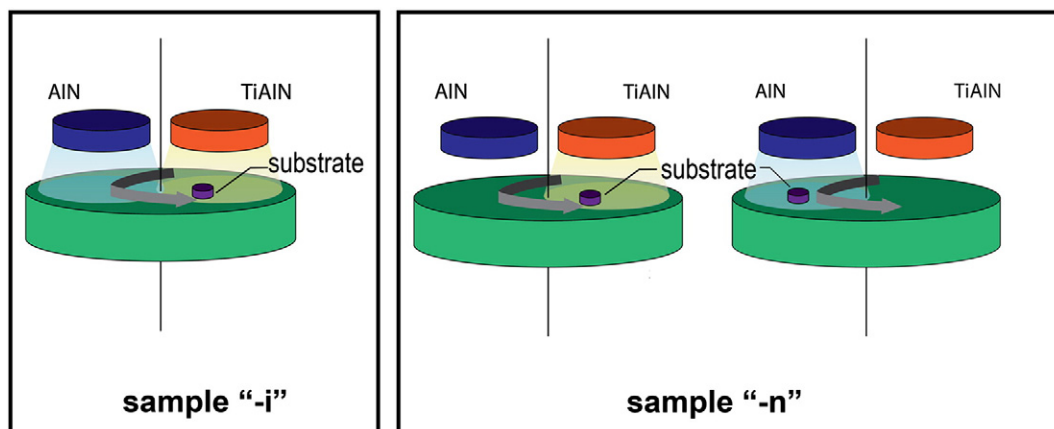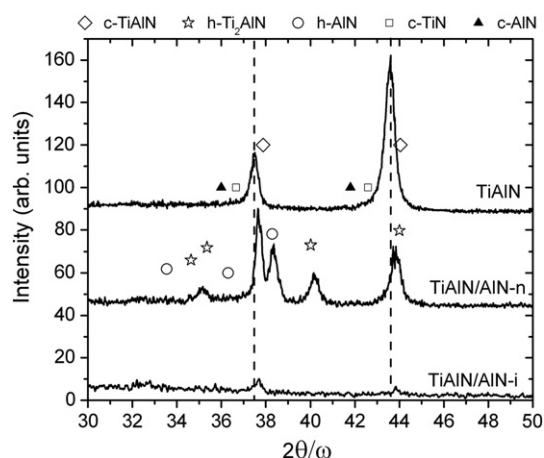

Fig. 1. Diagram of the deposition system and the relative positions of the target and the substrate. In this way it is easier to understand how the deposition was carried out for samples TiAlN/AlN-i and TiAlN/AlN-n.

Fig. 2. The X-ray diffractograms of TiAlN, TiAlN/AlN-n and TiAlN/AlN-i coatings. The symbols indicated in the legend of the figure correspond to the different phases present in the analyzed films.

crystallizes in the cubic NaCl modification (space group Fm3m) for AlN mole fractions x < 0.7 [15]. These latter peaks are present also in the diffractogram of the TiAlN single layer and the TiAlN/AlN-i multilayer (top and bottom of Fig. 2) where, however, the peaks corresponding to aluminum nitride phases are missing. The other symbols indicated in the legend correspond to the literature peak positions for cubic TiN, cubic AlN, hexagonal AlN and hexagonal Ti_2AlN [16]. The peak position of c-TiAlN (111) XRD reflection is equal to 37.46° for the single layer and becomes 37.71° for sample TiAlN/AlN-i while comes back to 37.63° for sample TiAlN/AlN-n. In the literature it is reported that the (111) diffraction peak shifts towards higher 2θ values at increasing aluminum content and then the two multilayers have a higher aluminum content with respect to the single layer, as expected by the growth deposition. Kutschej et al. in Ref. [17] assess that the incorporation of Al in the fcc $Ti_{1-x}Al_xN$ solid solution leads to a shift of the lattice parameter to lower values, caused by the substitution of Ti atoms by smaller Al atoms, and therefore to a significant shift of the fcc $Ti_{1-x}Al_xN$ peak to higher 2θ values compared to the standard position of TiN. According to the (111) c-TiAlN peak position of sample TiAlN/AlN-i, with respect to film TiAlN/AlN-n and to the single layer, we can say that sample -i has the higher Al content. Taking into account the dynamics of the deposition process we can conclude that when both targets are contemporarily swithced on, the formation of a TiAlN phase rich in aluminum takes place.

Instead, when the two targets are alternately shuttered, we assist to the formation of three phases: a cubic TiAlN phase with less aluminum content with respect to the other multilayer TiAlN/AlN-n but more aluminum content compared to the single layer TiAlN; a well separated AlN phase; and a second ternary phase like h-Ti2AlN richer in titanium. This can explain the XRD diffraction behavior of film TiAl/AlN-i.

XSR diffractogram [18] for the TiAlN/AlN-i coating shows only the interference due to the two film-substrate and film–air interfaces (Fig. 3a). In fact, a period equal to the thickness of the overall film is obtained (40 nm). A different spectrum is evidenced for sample TiAlN/AlN-n (Fig. 3b), whose reflectivity shows interfering peaks due to two different periodicities: the asterisks show the period of the alternation of the two layers (Λ = 4.28 nm) while the other peaks are due to the whole film thickness (D = 37.7 nm). These values agree with those obtained by the profilometer measurements of the total thickness and the number of rotations.

Therefore, the two deposition routines give rise to two structures with different stacking: TiAlN/AlN-n is a multilayered structure with an alternation of AlN and TiAlN films, on the other hand, TiAlN/AlN-i appears like a single film with only a cubic TiAlN phase with a level of order lower than the TiAlN reference sample.
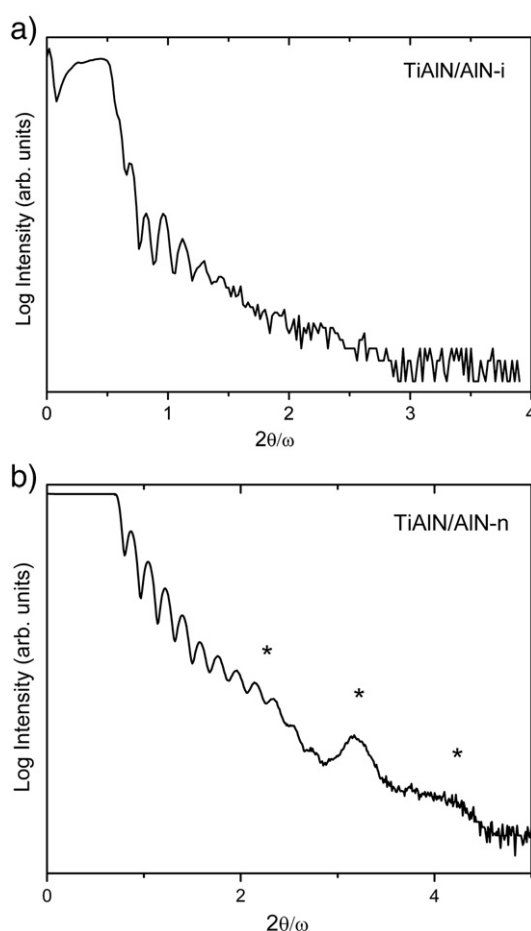
Fig. 3. XSR diffractograms for (a) the TiAlN/AlN-i coating and (b) the TiAlN/AlN-n coating. The dashed arrows indicate the frequency due to the whole film while the solid arrows show the period of the alternation of the two layers.

This suggests that the deposition approach used for the TiAlN/AlN-i sample gives rise to an intermixing of the different materials in each rotation cycle thus preventing the formation of nano-multilayer and also negatively affecting the crystalline quality of the film.

3.2. XPS results

The analyses of the surface region for the analyzed samples strongly reveal the presence of nitride species on both spectral regions of Ti 2p and Al 2p. After a peak fitting of the N 1s, Al 2p, Ti 2p and O 1s regions of a representative coating (see Fig. 4), the binding energy (BE) positions of the nitrides (on Ti 2p and Al 2p experimental peaks) result at lower values with respect to those predicted by the XPS NIST database [19] for the TiN and AlN single phases and those collected on reference samples [20].

In particular the N1s region (Fig. 4c) presents three different components: the first one (1) at 397.4 ± 0.2 eV, the second one (2) at 398.5 ± 0.2 eV and the third (3) at 400.7 ± 0.2 eV. They correspond to TiAlN and AlN compounds (1), TiON (2) and N_2 surface adsorbates (3), respectively. It can exclude the presence of TiN because no peak arises at 397 eV [21], as also confirmed by the absence of TiN peaks in the XRD analysis. A deconvolution of Al 2p region (Fig. 4b), with two unresolved 2p components, points out two sub-peaks: the first one at lower BE centered at 73.5 eV and another one at higher BE at 74.6 eV. Reminding that Al 2p line of AlN can be found in the range (74.3–74.7 eV) [19], the second component is undoubtedly attributed to AlN (together with a certain content of aluminum oxide as shown later in the test), while the first one could be
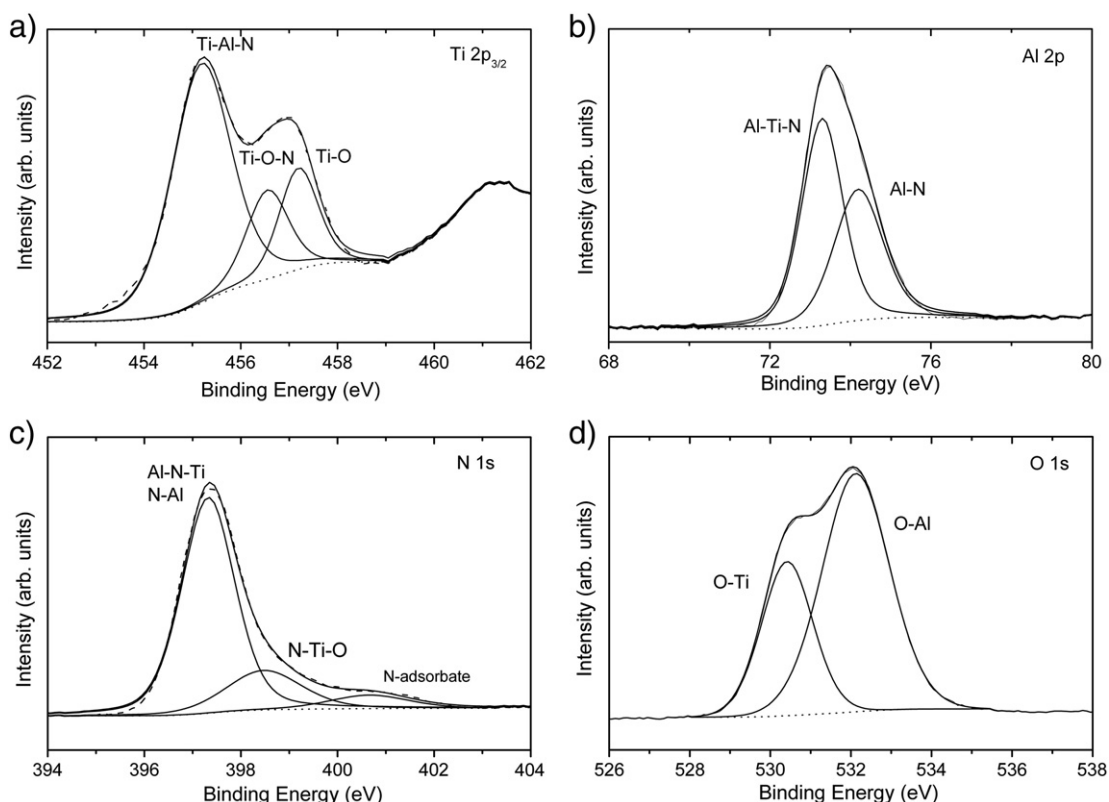
Fig. 4. XPS peak fittings of (a) Ti 2p, (b) Al 2p, (c) N 1s and (d) O 1s regions for a TiAlN/AlN-n representative coating.

attributed to AlN_x unstoichiometric compound, as Chen has interpreted [22], as well as to the TiAlN ternary compound. In our case the peak at 73.5 eV has been attributed to the ternary compound, because of the match with the peak position of the reference TiAlN single layer (see Fig. 5) and also because of the binding energy position read on Ti 2p region, recently attributed to the TiAlN compound [20].

As shown in Fig. 4a, three different components are revealed after peak fitting of the Ti $2p_{3/2}$ line: the first one at 455.0 eV is assigned to TiAlN and it is shifted of 0.3 eV towards low binding energy respect to the Ti $2p_{3/2}$ of the TiN compound acquired in our laboratories on samples deposited with the same technique [23]; the second one at 456.4 eV is attributed to TiO_xN_y compound; the third at 458.2 eV is identified as TiO_2.

O 1s after peak fitting (Fig. 4d) with the gaussian–lorentzian peak shape shows two different components: the first one at 530.4 eV associated to TiO_2 and the second one at 532.15 eV associated to aluminum oxide. The Al_2O_3 contribution is not well separated on Al 2p peak

Fig. 5. XPS Al 2p signal obtained for typical single layer TiAlN coating.

(Fig. 4b) because its energetic range (74.1–74. 6) eV falls in the same predicted for AlN. Therefore we do not exclude the presence of Al_2O_3 under the peak at 74.6 eV, that in literature has been uniquely attributed to Al_2O_3 [20]. The results of the XPS surface analyses are summarized in Table 1. Here there are the identification and the quantitative percentage for the different components of Ti2p3/2, Al 2p, N 1s and O 1s for the main analyzed typologies of samples: TiAlN single layer, TiAlN/AlN-i, and TiAlN/AlN-n.

As it can be noticed the reference single layer sample is a typical TiAlN coating with titanium native oxides on the surface region. In particular the Al 2p signal shows the unique presence of a TiAlN chemical environment (see Fig. 5). In the complex samples (TiAlN/AlN-i and TiAlN/AlN-n) the Al signal has been equally divided into two compounds, TiAlN and AlN, confirming what is expected by the growing procedure. Concerning the Ti 2p signal, it is evident that there is a very different quantitative distribution of the three compounds evidenced after the fit. The TiAlN/AlN-i sample is much more oxidized with respect to the other two samples. Results for the oxynitride components in table 1 for sample TiAlN/AlN-i were overestimated due to a resonance effect between the peaks associated to two different chemical titanium environments, as it has been presented by our structural analysis and supposed by Kutschej et al. in Ref. [17].

In order to get qualitative information inside the films, XPS measurements were taken at different depths through the coronene sputtering source, allowing depth profiling of the relative concentration of the four main elements in the films (Ti, Al, N, and O). The depth resolution at optimized operative parameters was about 10 nm, that is higher than the bilayer period, so it was not possible to calculate a reliable stoichiometry for each layer. As a consequence, the depth profiling allowed us to obtain an average concentration of the overall Ti, Al, N and O contents in the films. The average relative atomic percentage inside the single TiAlN film (spectrum not reported) was Ti 27%, Al 23%, N 48% and O 2%. In Fig. 6a and b the depth profiles for TiAlN/AlN-i and TiAlN/AlN-n samples are reported, indicating an overall composition of Ti 19%, Al 38%, N 39% and O 4% for sample TiAlN/AlN-i and Ti 23%, Al 40%, N 36%
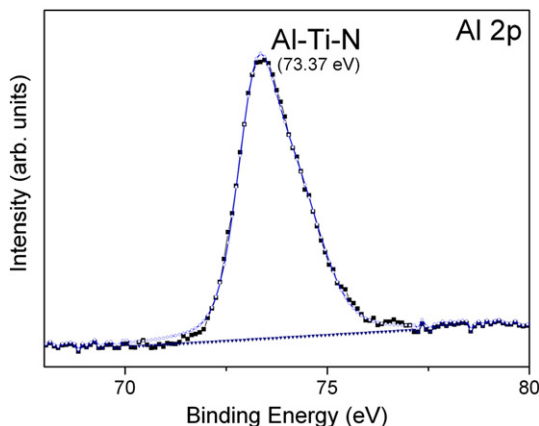
Table 1
The identification and the quantitative percentage for the different components of Ti $2p_{3/2}$, Al 2p, N 1s and O 1s for the main analyzed typologies of samples: TiAlN single layer, TiAlN/AlN-i, and TiAlN/AlN-n.

	Ti $2p_{3/2}$			Al 2p		N 1 s			O 1 s	
	Ti–Al–N at.%	Ti–O–N at.%	Ti–O at.%	Al–Ti–N at.%	Al–N at.%	N–Ti–Al at.%	N–Ti–O at.%	N_2 at.%	O–Ti at.%	O–Ti–N at.%
TiAlN	35	38	27	100	0	84	16	0	45	55
TiAlN/AlN-i	5	60	35	51	49	45	35	20	42	58
TiAlN/AlN-n	64	19	17	46	54	41	31	29	33	67

and O 1% for sample TiAlN/AlN-n. The nitrogen amount is lower than the overall metallic species contribution and, correspondingly, the amount of aluminum is always higher than titanium atomic percentage. It can be noticed that the overall Ti and Al percentages are about the same for both TiAlN/AlN samples, which is reasonable because both coatings are realized with the same deposition parameters (power, voltage and pressure). At the same time, the Ti and Al contents in these two films are respectively lower and higher than those in the single layer, as expected since in these two samples the Ti-containing layers (i.e. TiAlN layers) are alternated with AlN layers, thus giving a lower overall Ti percentage and higher overall Al percentage with respect to the single TiAlN layer.

The reported XPS average quantifications give place to a Ti/Al ratio around 0.5, depending on the architecture of the multilayers. This is in agreement with the XRD results, also in the case of sample TiAlN/AlN-n

where three distinct phases, Ti_2AlN, TiAlN aluminum-rich and AlN are identified, and XPS provides a chemical composition ratio Ti/Al < 1.

### 3.3. Thermal behavior of TiAlN/AlN multilayer coatings

Although the decomposition of metastable TiAlN with NaCl-type structure (c-TiAlN) upon annealing has been the subject of considerable research effort in the last decade [24–26], the structural evolution of films with mixed hexagonal Ti_2AlN and cubic TiAlN phases under annealing process is still little studied [27]. Then, according to the results of XRD investigation, the sample TiAlN/AlN-n appears more interesting than the other samples that showed peculiarities already known. The DTA curve for TiAlN/AlN-n coating, shown in Fig. 7a, evidences different peaks (labeled with numbers from 1 to 4) which indicate that several exothermic reactions occurred during annealing in Ar atmosphere from RT up to 1300 °C. XRD spectra taken after annealing at different temperatures can give information about physical transformations happening in the film. From the bottom to the top, Fig. 7b shows the GIXRD patterns for the film as-deposited and annealed at 700, 800, 900 and 1000 °C.

The diffractogram of the as-deposited sample clearly exhibits the presence of the cubic c-TiAlN and hexagonal h-Ti_2AlN ternary phases. Reflections in the vicinity of the theoretical positions of the h-AlN phase are also observed.

The two GIXRD patterns taken after annealing at 700 and 800 °C are very similar, as expected due to the absence of any significant reaction between these two temperatures in the DTA curve. These spectra show that: peaks at 35°, 40.2° and 44° associated to h-Ti_2AlN disappear as well as those associated to h-AlN; the c-TiAlN becomes sharper; three additional peaks at 39.2°, 42.3° and 43.4° appear but they do not match any previous reflection. The position and intensity of these peaks do not change at increasing the annealing temperature, indicating that this phase is thermally stable up to 1000 °C. Persson et al. [27] found a broad peak at 2θ = 38.5° indicative of the presence of intermetallic phases with residual Ti_2AlN content attributed to Ti_3Al and TiAl phases, in TiAlN coating realized at a substrate temperature of 1050 °C and lower nitrogen flux. Zhang et al. [28] realized films composed of Ti_2AlN and tetragonal Ti_2N phases (JCPDS Card No. 77-1893), finding that their phase structure did not change during annealing process, indicating phase stability of Ti_2AlN–Ti_2N during vacuum annealing at 800 °C. From the phase diagram, we get that for the above identified phases, TiAlN has tie lines with the intermetallics and Ti_2AlN, so it is natural for them to stay together in this material [29]. In our case the cubic phase c-TiAlN still remains after annealing at 700 °C, but the hexagonal phases h-AlN and h-Ti_2AlN have together given rise to an unique ternary phase rich in titanium and aluminum probably related to h-$Ti_3Al_2N_2$ phase. Reasonably the Ti in excess forms the tetragonal Ti_2N already observed at 700 °C [30]. The intermetallic phases are excluded in our identification, because the starting ternary compounds are not decomposable and the chemical bond with nitrogen is not broken at 700 °C.

(111) c-TiN reflection comes out at 900 °C, with its intensity increasing at increasing the annealing temperature. So after annealing at 1000 °C, TiN, Ti_2N, and $Ti_3Al_2N_2$ phases are copresent, as confirmed by the phase diagram [16].

From these observations, the peaks in Fig. 7a can be identified as follows: the first two peaks (1 and 2) are probably associated to an

a)

b)
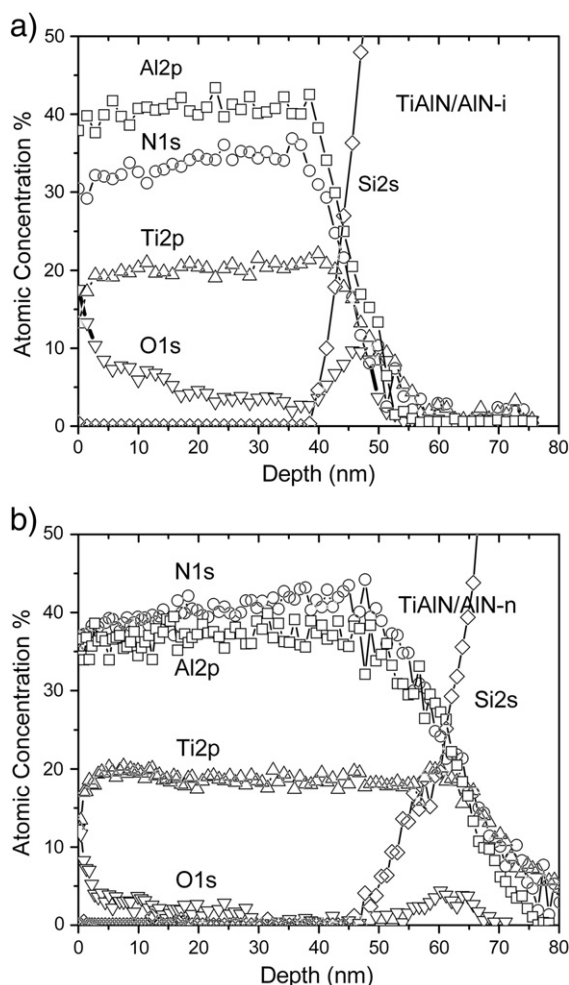
Fig. 6. XPS depth profiles for TiAlN/AlN-i and TiAlN/AlN-n films obtained using $C_{24}H_{12}^+$ (coronene) as sputtering source.
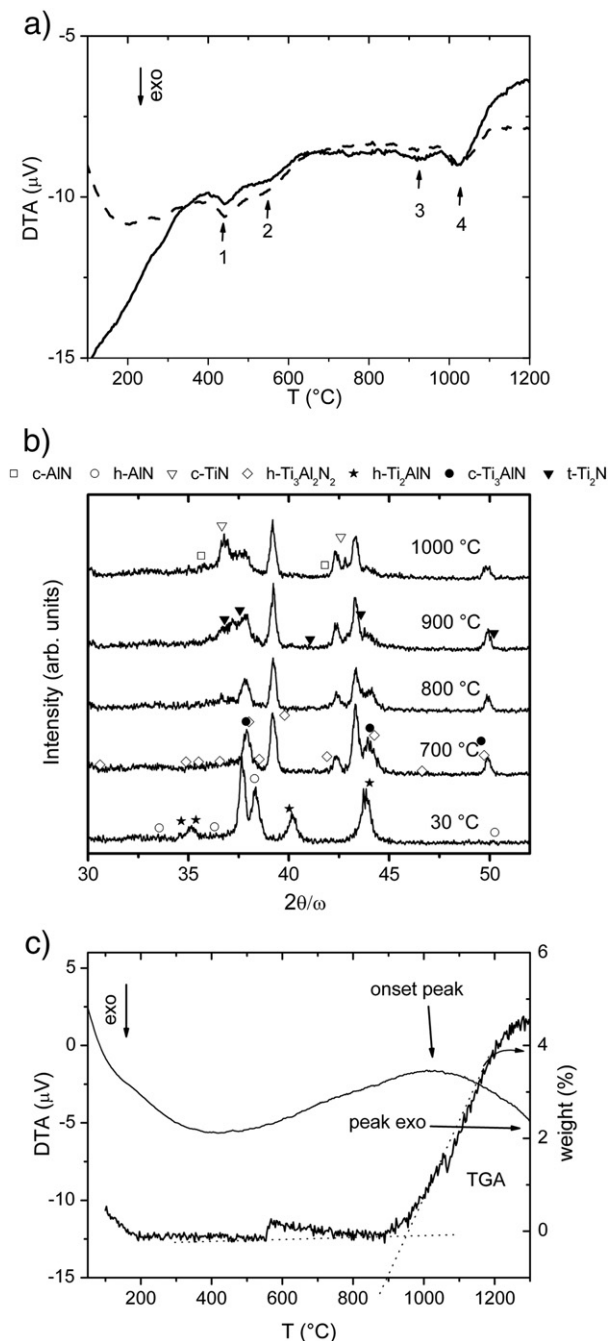
Fig. 7. a) DTA signal for sample TiAlN/AlN-n in flowing Ar. (b) GIXRD spectra of the sample as-deposited and after annealing at different temperatures. (c) DTA and TGA in flowing synthetic air.

initial recovery process of deposition-induced lattice point defects, followed by the disappearance of the AlN phase and the formation of the new $Ti_3Al_2N_2$ ternary phase; the third one (3) is related to the appearance of Ti_2N domains; finally, the last peak (4) shows the appearance of cubic TiN.

In Fig. 7c the DTA curve is pictured for the representative TiAlN/AlN-n coating after annealing in synthetic air up to 1300 °C. DTA signal is not corrected by baseline because its signal is very low and it is comparable to the error introduced by its correction. It exhibits an onset of the pronounced exothermic peak due to oxidation at temperature higher than 900 °C, hence, at least 400 °C above the oxidation temperature of TiN coatings. This information is more evident in the TGA signal compared to the DTA curve. The excellent oxidation resistance is confirmed by the preliminary results obtained by Wang et al. [31] on Ti_2AlN coatings.

3.4. Friction and wear

Single layer, intermixed-multilayer and nanolayered coatings deposited on WC–6%Co inserts have undergone wear tests at 30 °C and 400 °C.

The wear volume was assessed through the evaluation of the removed material section area, by a high precision profilometer, multiplied by the wear length. The average of 5 measurements for each track is here reported. Uncoated WC–6%Co insert has been used as reference sample for the tests. In Table 2 tribological test results are reported at two different temperatures: 30 °C and 400 °C. The values reported are the average of the experimental results. At 30 °C the friction coefficient μ is equal to 0.64 for the substrate inserts, while it decreases going down to a value 0.56 for the single layers, 0.54 for TiAlN/AlN-i and to 0.42 for the TiAlN/AlN-n coatings. The decreasing of the friction coefficient is already a very important result, but the tests performed on complex samples at high temperature (400 °C) evidenced even more interesting features. Fig. 8 represents the average friction coefficient of coatings as a function of the wear distance against steel balls at the temperature of 400 °C for all the representative samples. The friction coefficient for all samples has a very low value; a possible reason is the low normal load (1 N), which was used for the measurements and the low average value of surface roughness. The average RMS surface roughness is about 3.5 nm. For TiAlN single layer it appears clear that after 25 m a delamination occurred with sudden removal of the coating. This may suggest a weakness in term of adhesion between coating and substrate for this kind of coating. Friction coefficient of the coating is assessed where a clear contact between steel ball and coating occurred. Still it is very interesting the reduction of friction before delamination. The behavior for coating TiAlN/AlN-i appears more regular with a lower friction coefficient and a contact morphology less sensitive to loads, with an evident better adhesion between coating and substrate respect to the single layer. A small variation in the friction coefficient shows the presence of interaction between steel ball and coating. The TiAlN/AlN-n coating friction coefficient is very low indicating a smooth surface and suggesting a gradual exfoliation typical of the laminated structure.
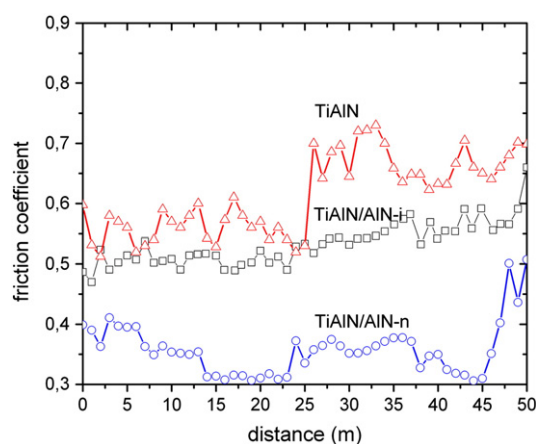
Summarizing the results, the friction coefficient increases to a value of 0.53 at 400 °C both for the single layer and the TiAl/AlN-i, while it decreases to 0.33 in the case of sample TiAl/AlN-n. A lower friction value indicates less adhesive areas between the ball and the surface of the tests, highlighting a different surface behavior of the two complex samples and giving the opportunity to better identify the kind of the wear mechanism. At the same time, the wear rate value is the highest in the bare substrate, while it is lower with the single layer coating and it further decreases to a limit value around 1.4×10^{-5} mm^3/N/m for the two complex sample typologies, indicating a better wear resistance in the case of the complex samples.

The SEM observations after wear tests at 400 °C and in the damaged regions are useful to better understand the mechanisms happening during the wear tests at the microscopic level. Fig. 9 shows the back-scattered electrons (BSE) image for a wear track in the

Table 2

Wear rate and friction coefficient μ, together with their corresponding standard deviation σ, at temperature of 30 °C and 400 °C.

Sample	T °C	Wear rate (mm^3/N/m) $\times 10^{-5}$	σ_{WR} (mm^3/N/m) x 10^{-6}	μ	σ_μ
TiAlN	30	5.11	3	0.56	0.026
	400	8.89	2	0.54	0.024
TiAlN/AlN-n	30	4.41	5	0.42	0.023
	400	1.35	5	0.33	0.020
TiAlN/AlN-i	30	4.19	4	0.54	0.018
	400	1.42	5	0.53	0.025
WC–Co	30	15.8	3	0.64	0.026
	400	19	5	0.66	0.025

Fig. 8. The average friction coefficient of coatings as a function of the wear distance against steel balls at the temperature of 400 °C for all the representative samples.

single TiAlN layer, where different shades of gray show a different chemical composition: the lightest areas (with greater average atomic number) represent the substrate while the darkest correspond to the film. EDS analysis performed inside the groove (labeled with a black circle in the left side of Fig. 9) reveals a composition corresponding to the WC–6%Co substrate, therefore indicating a complete removal of the TiAlN coating (white circle). The inset at the top right of Fig. 9 shows a secondary electron (SE) image which highlights a borderline region with not well defined contours, from where a certain number of cracks start to propagate onto the coating surface. Although the load was very weak the material is very fragile and not tough, so that it can be spoken of as having "brittle failure wear".

In Fig. 10 the SEM image with SE (a) and with BSE (b) shows the surface region of a wear groove in the multilayer TiAlN/AlN-i. It is well evidenced that the groove region is not homogeneous and presents localized pits of about 50 μm. EDS analyses were performed at three different zones, labeled with x, y and z. Looking to the EDS peaks,

it can be concluded that the lighter zones (like x) are likely the substrate (flakings), the gray zone (y) is the remaining coating, and the darker zone (z) is that part of the coating containing the ferrous debris of the ball. Flakings are actually areas uncovered by the coating, especially in the aftermath of the wear test. It means that the initial impact created these delaminated areas, generally due to a surface fatigue phenomenon, with consequent release of small debris of the coating material which takes part of the subsequent erosion both of the surface and the ball. In this case, abrasive wear of three bodies interacting can be spoken of, where the debris formed in the initial phase of the test then contributes to abrasion. This situation is found every time there is a great difference between the hardness of the two bodies interacting. Although Fe was detected on the coating, there was no Al or Ti element on the abrasion mark of the steel ball. The debris layer and the obvious debris adherence represented the main characteristics of the wear track.

In Fig. 11 there is a comparison between the SEM image with SE (a) and BSE (b), for the same groove considered for sample TiAlN/AlN-n. It can be observed that there are many areas within the groove where the film has not been completely removed, even after 500 cycles. It drives towards the abrasive wear where, at the same working conditions, the film can be removed with more difficulty. In Fig. 11c a detail of the same groove is considered. The groove generated by the wear test has a well defined and delimited contour (right side of the image) and also the wall section of the coating is well visible and presents a certain number of overlayered slides (Fig. 11d), indicating the multilayered structure of the coating. Precisely this laminar structure is probably linked to the lower value of the coefficient of friction.

4. Summary and conclusions

Single layer, intermixed-multilayer, and nanolayered coatings of TiAlN/AlN were fabricated using reactive magnetron sputtering in Ar and N_2 gas mixture. The experimental results can be summarized as follow:
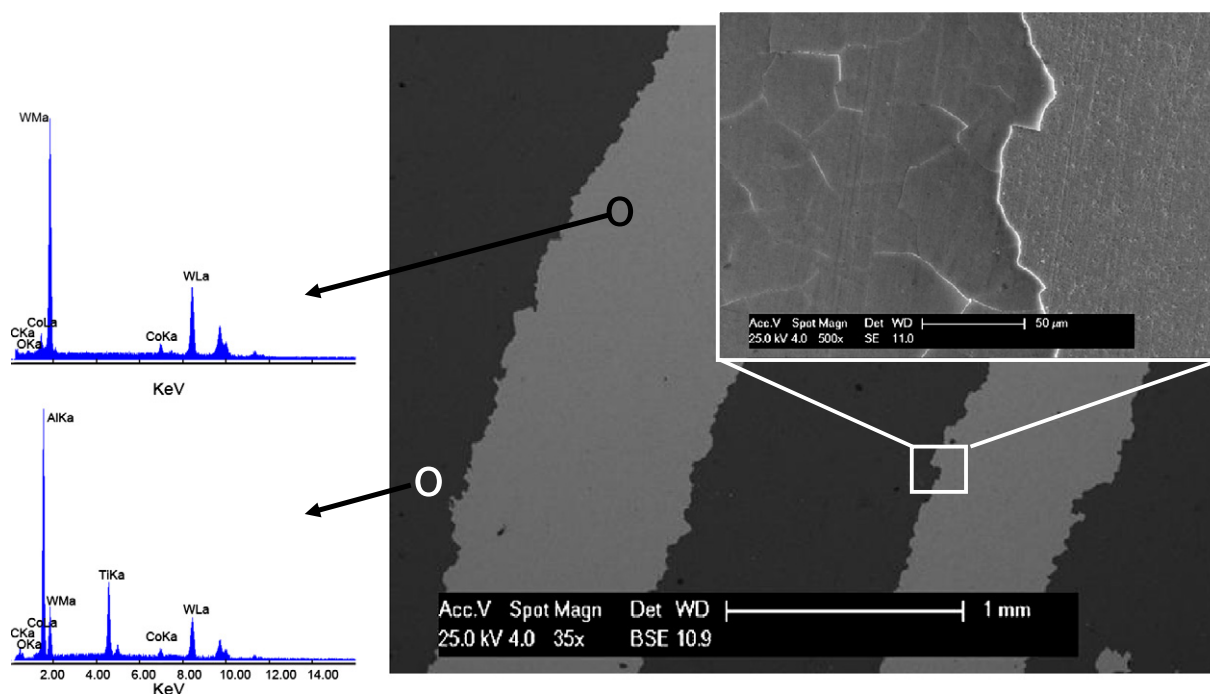

Fig. 9. Worn surface BSE micrograph of single layer TiAlN deposited on WC–6%Co after wear test at 400 °C. At the left side, EDS analyses performed inside the groove (labeled with a black circle) and on the TiAlN (labeled with a white circle). At the top right there is a particular zone at higher magnification taken with SE, that shows a certain number of cracks onto the coating surface.
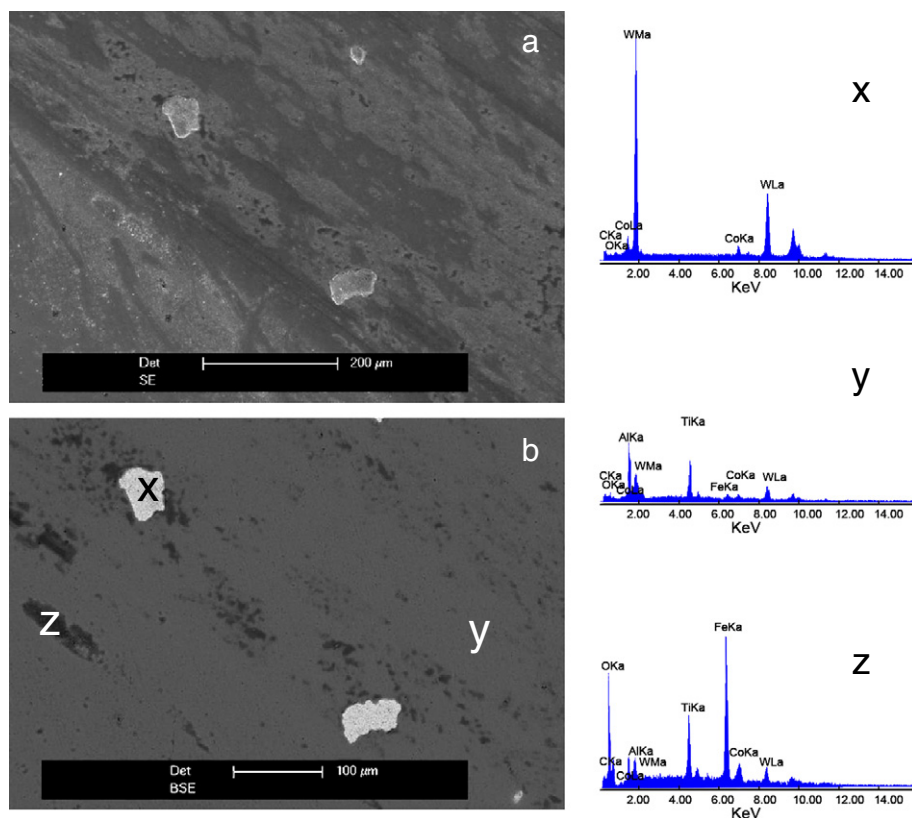
Fig. 10. SEM image with SE (a) and with BSE (b) relative to a surface region of a wear groove for the multilayer TiAlN/AlN-i. At the right side EDS analyses performed inside the groove in three different points labeled with x, y and z.
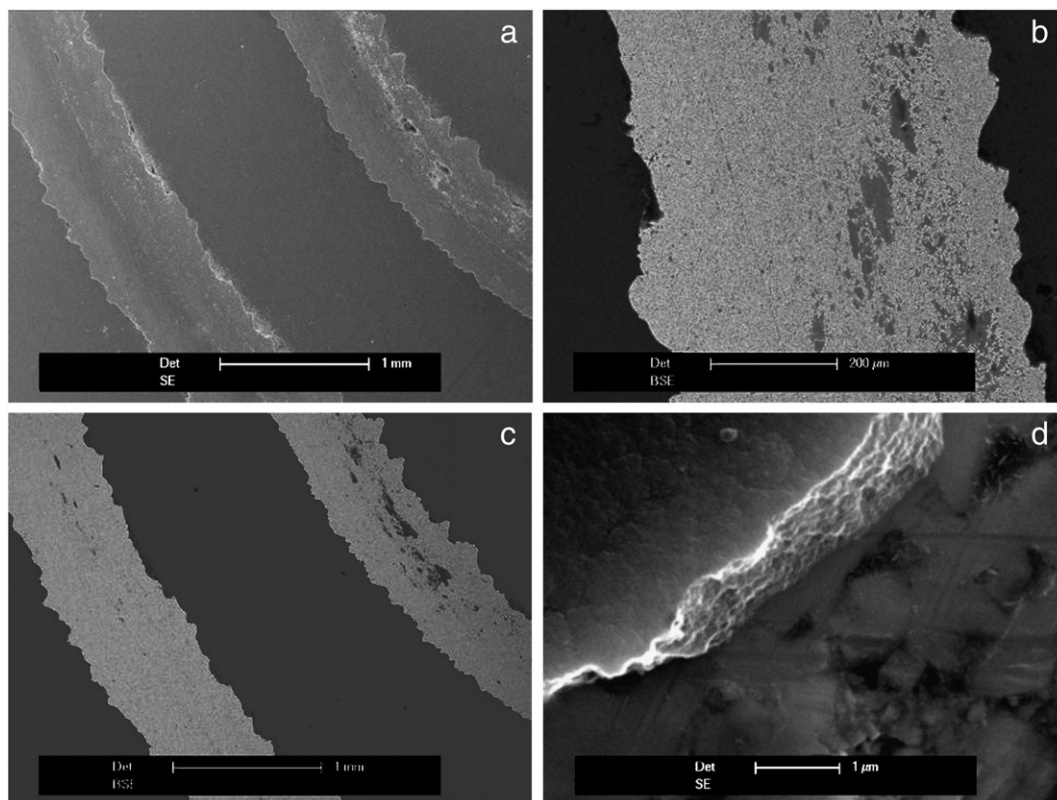
Fig. 11. SEM image with SE (a) and BSE (b) of the same groove for sample TiAlN/AlN-n. (c) and (d) Details of the same groove.

1. XRD examinations revealed that TiAlN single layer had a cubic structure of TiAlN with (111) preferential orientation. The Al 2p XPS surface spectrum consisted of only one peak at 73.5 eV attributed to the ternary nitride titanium aluminum compound. The surface Ti $2p_{3/2}$ peak presents, apart the oxide and oxynitride components, a clear component attributed to the nitride titanium aluminum compound. The relative atomic percentage inside the single TiAlN film was: Ti 27%, Al 23%, N 48% and O 2%. TiAlN single layer showed a brittle failure wear in fact, at 400 °C and a weak load of 1 N applied, wear test grooves showed regions where the coating was completely removed.

2. TiAlN/AlN-i has been realized by continuous deposition with both targets (TiAl and Al) turned on and the substrate that rotates and passes under each of the targets. TiAlN/AlN-i appears like a single film with the two materials intermixed, forming only a cubic TiAlN phase with a level of order less than the TiAlN reference sample but more rich in aluminum. The XPS Al 2p signal consisted of two peaks: the first one at 73.5 eV attributed to the ternary nitride titanium aluminum compound and the other one at higher BE at 74.6 eV attributed to AlN. The depth profile indicates the overall composition for the main elements inside the coatings: Ti 19%, Al 38%, N 39% and O 4%.

3. The multilayer TiAlN/AlN-n was realized with only one target alternatively shuttered. The XPS Al signal has been equally divided into two compounds, TiAlN and AlN, confirming what was expected by the growing procedure. The depth profile indicates the overall composition for the main elements of the coatings, that is: Ti 23% Al 40% N 36% and O 1%. TiAlN/AlN-n is a multilayered structure with an alternation of AlN and TiAlN films where there is evidence of hexagonal AlN phase besides the ternary phases of hexagonal Ti_2AlN and cubic aluminum rich-TiAlN.

DTA results indicate that several exothermic reactions occur during annealing in Ar atmosphere from RT up to 1300 °C. XRD after annealing at temperatures corresponding to exothermic peaks' position has allowed the identification of peaks: the first two peaks are probably associated to an initial recovery process of deposition-induced lattice point defects, followed by the disappearance of the AlN phase and the formation of the new $Ti_3Al_2N_2$ ternary phase; the third one is related to the appearance of Ti_2N domains; the last peak shows the appearance of cubic TiN. The films exhibited excellent oxidation resistance and thermal stability at 900 °C in air. Compared with other coatings, the multilayered coated samples presented better wear resistance properties, due to structure stability and coating design features. In the case of sample TiAl/AlN-n the friction coefficient has a lower value of 0.33 at 400° with respect to the value 0.53 both for the single layer and the TiAl/AlN-i. A lower friction value indicates less adhesive areas between the ball and the surface of the coatings, highlighting a different surface behavior of the two complex samples. Moreover TiAlN/AlN-n presented a better wear resistance than the other typologies of films. This behavior can be associated to the presence of interfaces: since each interface becomes an obstacle to the crack propagation, a better wear resistance was registered for smooth surface and hard multilayered coatings.

References

[1] W. Grzesik, P. Nieslony, Wear 256 (2004) 108.
[2] G.M. Robinson, M.J. Jackson, M.D. Whitfield, J. Mater. Sci. 42 (2007) 2002.
[3] M. Kathrein, C. Michotte, M. Penoy, P. polcik, C. Mitter, Surf. Coat. Technol. 200 (2005) 1867.
[4] S.Y. Yoon, J.K. Kim, K.H. Kim, Surf. Coat. Technol. 161 (2002) 237.
[5] D. Mclntyre, J.E. Greene, G. Hakansson, J. Sundgren, W.D. Eand Munz, J. Appl. Phys. 67 (1990) 1542.
[6] J. Musil, H. Hrubý, Thin Solid Films 365 (2000) 104.
[7] J.-L. Huang, B.-Y. Shew, J. Am. Ceram. Soc. 82 (1999) 696.
[8] Z. Zhou, W.M. Rainforth, Q. Luo, P.Eh. Hovsepian, J.J. Ojeda, M.E. Romero-Gonzalez, Acta Mater. 58 (2010) 2912.
[9] E. Voglia, W. Tillmannb, U. Selvadurai-Lasslb, G. Fischerb, J. Herper, Appl. Surf. Sci. 257 (2011) 8550.
[10] L. Chen, Y. Du, X. Xiong, K.K. Chang, M.J. Wu, Int. J. Refract. Met. Hard Mater 29 (2011) 68.
[11] L. Chen, Y. Du, P.H. Mayrhofer, S.Q. Wang, J. Li, Surf. Coat. Technol. 202 (2008) 5158.
[12] L. Chen, M. Moser, Y. Du, P.H. Mayrhofer, Thin Solid Films 517 (2009) 6635.
[13] A. Rafat, M.C. Davies, A.G. Shard, S. Hutton, G. Mishra, M.R. Alexande, J. Controlled Release 139 (2009) 40.
[14] www.casaxps.com.
[15] T. Ikeda, H. Sato, Thin Solid Films 195 (1991) 99.
[16] Y.S. Han, K.B. Kalmykov, S.F. Dunaev, A.I. Zaitsev, J. Phase Equilib. Diffus. 25 (2004) 427.
[17] K. Kutschej, P.H. Mayrhofer, M. Kathrein, P. Polcik, R. Tessadri, C. Mitterer, Surf. Coat. Technol. 200 (2005) 2358.
[18] E.E. Fullerton, I.K. Schuller, H. Vanderstraeten, Y. Bruynseraede, Phys. Rev. B 45 (1992) 9292.
[19] www.nistgov.com.
[20] M. Čekada, Surface properties and engineering of complex intermetallics, Cap 1, pag.1 © World Scientific Publishing Co. Pte. Ltd., http://www.worldscibooks.com/physics/7733.html.
[21] J.F. Marco, J.R. Gancedo, M.A. Auger, O. Sanchez, J.M. Albella, Surf. Interface Anal. 37 (2005) 1082.
[22] J.T. Chen, J. Wang, F. Zhang, G.A. Zhang, X.Y. Fan, Z.G. Wu, P.X. Yan, J. Alloys Compd. 472 (2009) 91.
[23] A. Rizzo, M.A. Signore, L. Mirenghi, T. Di Luccio, Thin Solid Films 517 (2009) 5956.
[24] A. Knutsson, M.P. Johansson, P.O.Å. Persson, L. Hultman, M. Odén, Appl. Phys. Lett. 93 (2008) 143110.
[25] P.H. Mayrhofer, A. Hörling, L. Karlsson, J. Sjölen, T. Larsson, C. Mitterer, L. Hultman, Appl. Phys. Lett. 83 (2003) 2049.
[26] P.H. Mayrhofer, D. Music, J.M. Schneider, Appl. Phys. Lett. 88 (2006) 071922.
[27] P.O.Å. Persson, S. Kodambak, I. Petrov, L. Hultman, Acta Mater. 55 (2007) 4401.
[28] T.F. Zhang, Q.M. Wang, J.L. Peiling Ke, R. Nowak, K. Ho Kim, Surf. Coat. Technol. 212 (2012) 199.
[29] T. Joelsson, A. Flink, J. Birch, L. Hultman, J. Appl. Phys. 102 (2007) 074918.
[30] T. Ikeda, H. Sato, Thin Solid Films 195 (1991) 99.
[31] Q.M. Wang, W. Garkas, A. Flores Renteria, C. Leyens, K.H. Kim, J. Nanosci. Nanotechnol. 11 (2011) 8959.